Article

Thermal Stability of Sputtered Tungsten Nitrides for Solar Thermal Applications

Anna Castaldo [1,*] **, Emilia Gambale** [1] **and Laura Iemmo** [2]

1   ENEA, TERIN-STSN-SCIS, Piazzale Enrico Fermi 1, 80055 Portici, Italy
2   Physics Department "E.R. Caianiello", University of Salerno, Via Giovanni Paolo II, 132, 84084 Fisciano, Italy
*   Correspondence: anna.castaldo@enea.it; Tel.: +39-(0)817723358

Featured Application: This work describes the thermal stability of thin films of tungsten nitrides in vacuum and can be useful in solar thermodynamic field for tailoring solar absorbers, capacitive energy storage devices and catalysts for hydrogen evolution reaction, and in fusion applications for plasma facing materials.

Abstract: In this work, tungsten nitrides sputtered at different powers supplied to a W target (300 W, 500 W, 700 W) and proposed for solar thermal applications as part of solar absorbers, as active and robust materials for capacity energy storage and as plasma-facing materials were annealed in vacuum at medium-high temperatures (470 °C, 580 °C) and characterized by means of X-ray diffraction (XRD), AFM, micro-Raman, FTIR, UV–VIS—NIR, sheet, surficial energy and wetting angle measurements. From the overall set of analyses, some important modifications and differences between samples after annealing emerged (which will be useful for selecting them for specific applications) and have been correlated to sputtered W metallic clusters' ability to adsorb, form complexes with and react with the strong N_2 triple bond under the various plasma conditions of a reactive sputtering process. In particular, the 300 W film of poor crystalline quality as deposited, after annealing released entrapped nitrogen and retained its W_2N structure up to a temperature of 580 °C. Despite there being no phase transition, there was an increase in sheet resistance, which is detrimental because the preservation of metallic character is an important requisite for the proposed applications. The 500 W film had a stable crystalline structure and a metallic character unmodified by increasing temperature. The 700 W film, whose structure as deposited was almost amorphous, underwent the most severe modification after annealing: crystallizing, disproportioning and giving rise to a composite and porous nature $(W + WN_x)$ not ideal for spectrally selective coating applications, but useful for tailoring capacitive energy storage devices, or for catalysts for hydrogen evolution reactions (as an alternative to platinum) in alkaline water electrolysis.

Keywords: spectrally selective coatings; reactive sputtering; transition metals nitrides; solar absorbers; cermet; catalysts; annealing; capacitive energy storage

1. Introduction

Heat collecting elements utilize spectrally selective tailored metamaterials (deposited as multi-layered coatings on stainless steel tubular substrates) for absorbing solar energy and transferring it to thermo-vector fluids (e.g., molten salts, diathermic oil) which feed thermodynamic cycles to obtain high temperature heat or electrical power (CSP technology) [1]. Various metamaterials have been developed and optimized for use in receiver plants operating at medium (673 K) and high (823 K) temperatures [2]. In particular, cermet-based nitride multilayers containing tungsten nitrides as metallic component in an insulating matrix of aluminium nitride, both materials being deposited by reactive dc magnetron co-sputtering in an Ar-N_2 gas mixture [3], have been used as absorbers in spectrally selective coatings of a receiver tube in molten salt plants, demonstrating very

good performance in terms of photo-thermal conversion of solar energy [4]. The choice of tungsten nitrides as constituents of double nitride cermet is due to their metallic behavior and to the scarce wettability of these compounds with the ceramic insulating AlN matrix, useful for spheroidizing the metallic component during the co-sputtering fabrication process and hence obtaining a good cermet. The whole process of "double nitride" formulation has been based on the chemistry of simultaneous nitridation of transition and earth alkaline metals [5].

Tungsten nitrides being a large family of compounds, their properties depend on the exact stoichiometry [6] and phase. Their crystal structure consists of a fcc sub-lattice of W atoms. Half the octahedral holes are filled with N atoms in the β-W_2N structure. All the octahedral holes are filled with nitrogen in the δ-WN structure. These arrangements produce a cubic crystal lattice for β-W_2N and a hexagonal lattice structure for δ-WN. Extra N atoms occur at grain boundaries between tungsten nitride crystallites. In Table 1, various structure types and phases are reported.

Table 1. Phases of tungsten nitride and their structure types.

Phase	Structure Type
α-W_xN	solid solution of N in α-tungsten
β-W_2N	cubic face centred
γ-WN	tetragonal
γ-W_3N_4	cubic
δ-WN	hexagonal
WN_2 insulating (WO_3 if exposed to the air)	rhombohedral

As the receiver fabrication technology requires that the spectral selective coating works under a good vacuum at medium-to-high temperatures (673 K for diatermic oil plants, 823 K for molten salts ones), it needs a very high structural, physical and chemical stability in these conditions, without modification of the double nitride (AlN–WN) optical properties due to phase transitions of the constituents. In consideration of the fact that the cermet matrix AlN has already been well characterized [7] and the influence of process parameter on fabrication of WN has been the topic of a previous work [8], the aim of this paper is to add new studies on the thermal stability of tungsten nitride in vacuum. The thermal stability in air of thin films of tungsten nitrides and their characteristic nitrogen loss have been studied at temperatures of 473 K, 673 K and 873 K by Answar [9] with the aim of using these materials as diffusion barriers in microelectronics or as electrodes in semiconductor devices, and by Abdelhameed and Jacob [10] at temperatures of 1200 K for investigating nitrogen release.

Moreover, tungsten nitrides have been attracting a lot of attention in other applications, such as water reduction catalysts in hydrogen production water splitting processes; for promoting hydrogen evolution reactions (HER) in alkaline media, replacing the much more expensive platinum [11]; as material for capacitive energy storage devices [12]; and for plasma facing material for fusion applications [13].

For example, in catalyst applications it is important to achieve a balance between electrical conductivity and energetics of absorption/desorption of reaction intermediates in HER activities, both being related (albeit inversely) to nitrogen content [14]. In this field, it can also be interesting to increase the density of active sites and to test conductivity and stability at high temperatures. As shown in the work mentioned above [8], which investigated the process parameters of tungsten nitrides' sputtering deposition, it is possible to obtain different WN_x phases over a large composition range of x (from 0.5 to 2.0) and changes in electrical properties from conductive to insulating ones. Taking into account that the thermal stability of tungsten nitrides can be crucial for their use both in spectrally selective coatings for receiver tube of CSP plants and for other applications, this study

presents a combined analysis of the structural, vibrational and optical properties of thin WN_x films after annealing at two different temperatures (470 °C and 580 °C), considered useful for the employment of such materials.

2. Materials and Methods

Tungsten nitride thin films were deposited by DC-pulsed reactive sputtering using a planar magnetron sputtering deposition apparatus from Material Research Corporation mod. MRC 643. Substrates, maintained at floating potential, were mounted on a holder that moved back and forth in relation to the tungsten target (12 cm × 38 cm, 99.95 % of purity) with a sweep velocity of 200 cm/min and substrate–target distance of 80 mm. All samples were fabricated starting from a base vacuum condition of approximately 2×10^{-4} Pa. The films were produced in an argon/nitrogen atmosphere with 14% nitrogen concentration in the sputtering gas, at a total deposition pressure of 0.73 Pa and at three power densities applied to the target: 300 W, 500 W and 700 W. The frequency and the on–off time of the DC pulsed generator were 230 KHz and 1.9 µs, respectively. The thickness of films was measured using a KLA Tencor P-10 surface mechanical profiler manufactured by KLA Corporation. 1 Technology Drive, Milpitas, CA 95035, USA and their sheet resistance values were determined by means of the four points technique, using a Napson Resistest mod. RT-8A. UV–VIS–NIR reflectance curves were obtained by a double-beam Perkin-Elmer mod. Lambda 900 instrument, equipped with a 10 cm diameter integrating sphere.

Aluminium nitride-based cermets containing WN 300 W, 500 W and 700 W were produced by means of reactive co-sputtering processes, where the power supplied to the aluminium target was 3000 W.

X-ray diffraction (XRD) analysis was performed with a Philips X'Pert PRO MRD diffractometer (manufactured by Philips Lelyweg 1 7602 EA Almelo The Netherlands.) working with CuKα radiation (λ = 0.154056 nm), using a grazing incidence angle of 1.5°. A scan range of 10–95° (2θ) was used. The diffraction data were used to calculate the crystallite size of the films using Scherrer's formula, d = λ/(β cos θ), where λ is the wavelength of the X-ray used, β is the full-width half maximum measured at the θ value of the peak. The morphology and the structure of the films were evaluated by AFM. Raman scattering experiments were performed using a micro-Raman system (inVia model of Renishaw) at room temperature, using as excitation the 514 nm line of an Ar ion laser at normal incidence. The nominal laser power used in these measurements was 20 mW. Typical spectrum acquisition time was limited to 50 s to minimize the sample heating. FTIR reflectance spectra were recorded on a Bruker Fourier transform instrument spectrometer (model Equinox 55), equipped with an integrating sphere and a MCT detector operating in the range 570–8000 cm^{-1}. A resolution of 8 cm^{-1} was utilized. FTIR transmittance spectra were recorded with a Perkin Elmer Fourier transform instrument spectrometer equipped with a Deuterated Triglycine Sulfate (DTGS) detector operating in the 400–10,000 cm^{-1}, with a resolution of 2 cm^{-1}.

The sessile drop method was used for measuring wetting behavior at room temperature, by means of a KRUSS DSA 100 instrument. Water and di-iodomethane small liquid droplets (6 µL) were formed on the end of the disposable needle (stainless steel, with a PP luer-lock connector, with a length of 38 mm and a diameter of 0.5 mm; Krüss NE 44), which were then carefully deposited onto the films' surface. Digital images of the droplet silhouette were captured with a high-quality camera, followed by the contact angle determination by numerically fitting the droplet image. The values reported herein are the average of at least five measurements on various parts of each sample.

3. Results

The fabrication of tungsten nitrides by means of reactive sputtering has been the topic of a previous study on the influence of the deposition power and nitrogen content on the properties of thin films as they are grown. Large variation in the electrical resistivity as a function of the power supplied to the W target has been observed, in the direction of an

increase of metallic character with power, as expected in different regimes of operating target during nitridation. The metallic character of WN films increases and the crystal content decreases with increasing deposition power from 300 to 700 W. In particular, from a structural point of view, the 300 W film is crystalline with a cubic distorted lattice of W_2N hosting nitrogen in interstitial sites. The 500 W target power determines a highly crystalline growth of W_2N with a small amount of amorphous phase. When power is increased to 700 W, an amorphous phase appears together with the W_2N phase. This behavior has been defined as an effect of re-sputtering phenomena that occur at higher powers. Stability being an important requisite of a solar thermodynamic coating, the object of previous work has been to select ideal experimental conditions for maximizing the content of a thermodynamically stable fcc phase of W_2N. In any case, the various phases—and in particular δ-WN and the porous nitrides brought about when nitrogen is in excess—seem to have better catalytic performance in HER [15]. Moreover, there are material applications where different phases coexist, for example, the graded cermet AlN–WN, utilized as an absorber in the spectrally selective double nitride coating previously mentioned. In the optimized reactive co-sputtering cermet fabrication process, starting from 700 W (used for the cermet layer in proximity to the metallic back reflector) and arriving at 300 W (used in the fabrication of cermet of low metallic content in proximity to the antireflective layer) various powers are supplied to the W target. This means that different WN_x phases can be originated and extra N atoms can be entrapped in lattices and/or at grain boundaries of these graded double nitride absorbers. For the purpose of studying the stability of tungsten nitride particles inside graded cermet in operating conditions of receiver tubes, single tungsten nitrides films, WN_x, and thin films of AlN–WN cermet at three different powers (300 W, 500 W and 700 W) were produced, vacuum annealed and characterized. It is important to outline that the samples deposited at 300, 500, and 700 W were all of a similar thickness (about 100 nm).

Single WN_x films were subjected to two consecutive thermal treatments, at 470 °C for 8 h and at 580 °C for 6 h in vacuum, and studied for the application of receiver tubes at medium (400 °C) and high (550 °C) temperatures, for the purpose of verifying the materials' thermal stability and to promote gas-entrapped desorption.

The sheet resistance (Figure 1) of the 300 W film increased after annealing, suggesting the film's less conductive nature after annealing. In the 500 W and 700 W films, sheet resistance remained almost unchanged.
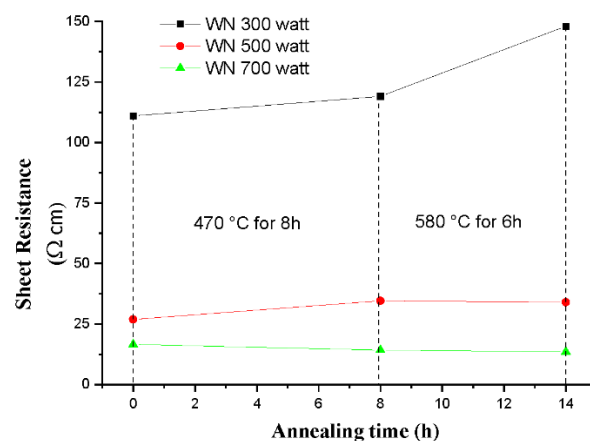

Figure 1. Sheet resistance versus annealing time.

The UV–VIS–NIR reflectance spectra analysis of films before and after the two annealing steps (Figure 2) shows that there were modifications in the optical films' properties. Such modifications were produced by the first annealing in the case of 300 W and 500 W, and were progressive in the 700 W film. In particular, for 300 W, there was a 2% decrease in the NIR reflectance only, starting from 1500 nm, due to a decrease in its metallic character

(maybe due to W oxidation). For the 500 W and 700 W films, the prevalent modification occurred around 1000 nm but the overall reflectance diminished after annealing, which can be explained by the nitridation and/or oxidation of metallic tungsten by means of gases entrapped in the lattice or at grain boundaries and their subsequent release.
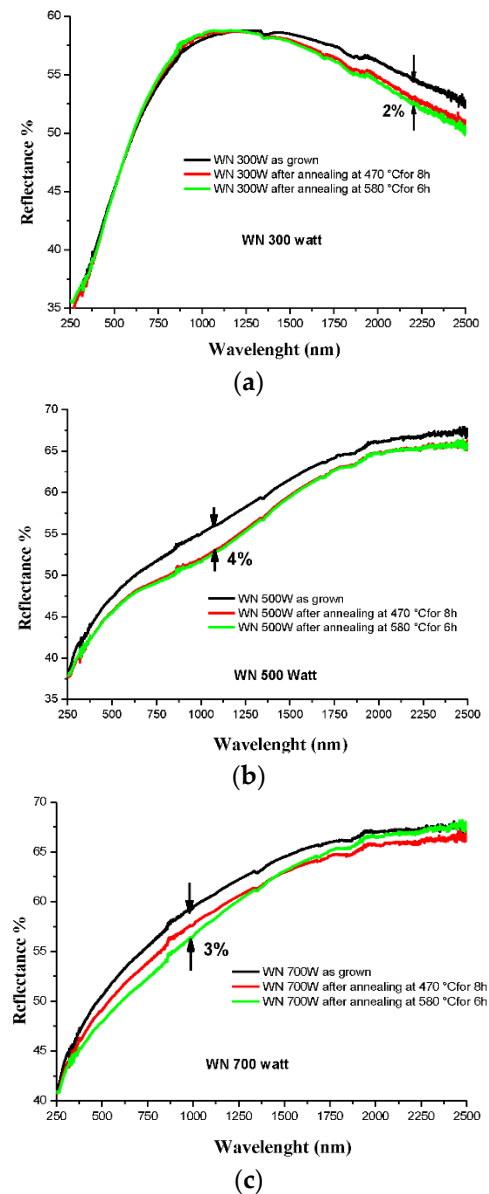

Figure 2. UV–VIS–NIR reflectance of (**a**) 300 W, (**b**) 500 W, (**c**) 700 W.

The X-ray diffraction peaks of reactively sputtered tungsten nitride, WN_x produced at different deposition powers are shown in Figure 3. Phases of the WN_x films before and after annealing at 470 °C and 580 °C were analyzed.

The "as grown" film produced at the lowest deposition power (300 W) exhibited a single fcc W_2N phase whose crystallinity increased with annealing. At 500 W, a poorly ordered W_2N phase mixed with an amorphous phase (identified by the deconvolution procedure as a broad peak around 2θ 37.7° and with a full width at half height (FWHM) at maximum of 5.2°) was observed, whereas at 700 W only a prevalent amorphous phase was present. The cubic β-W_2N phase had a (111) preferred orientation. The material deposited at 300 W, having a high nitridation level, exhibited the highest 2θ shift in the diffraction peaks with regards to the ICDD database position, which may be due to the release of stresses. When the deposition power increases, this phenomenon is less noticeable.
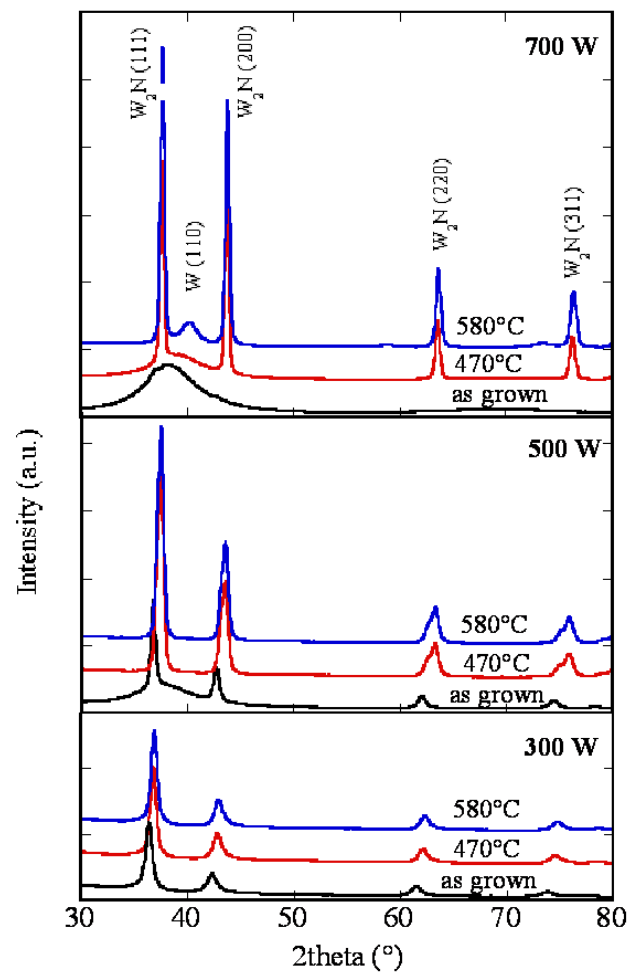
Figure 3. XRD patterns of different WN$_x$ films before and after annealing.

Related lattice parameters (see Figure 4) were higher than the corresponding bulk value of the W$_2$N phase (4.126 Å). The increase in the lattice constant can be attributed to the incorporation of excess nitrogen atoms that can occupy the vacant octahedral sites, resulting in the W$_2$N lattice's expansion [16]. The film deposited at lower deposition power consisted of small grains, whereas at higher deposition powers larger grains were present. Annealing of the deposited films resulted in an improved crystallinity of the W$_2$N grains and in a crystallization of the amorphous phase. The larger annealing effects on the crystallization could already observed at 470 °C; raising the temperature to 580 °C produced only a slight improvement in crystallinity.

At deposition powers of 300 and 500 W, only β-W$_2$N was present after annealing, whereas for the material obtained at 700 W, a two-phase structure of W$_2$N and bbc α-W appeared and the diffracted intensities increased at the higher annealing temperature. The modification seems to be progressive.

For the films obtained at a low deposition power (300 W), the preferential (111) orientation of the W$_2$N phase persisted after annealing, whereas when the deposition power was increased, the annealing produced not only large grains with a (111) preferential orientation, but also a further growth of grains with a (200) orientation. At a deposition power of 700 W, this effect was more pronounced. Interchanges from the preferred (111) direction to (200) have also been reported for thin niobium nitride films subjected to annealing [17]. Nitrogen readily chemisorbs on the (200) planes but not on the N-terminated (111) planes, which reduces the flux of cations in the (200) compared to the (111) planes, resulting in the orientation of growth in the (200) direction.
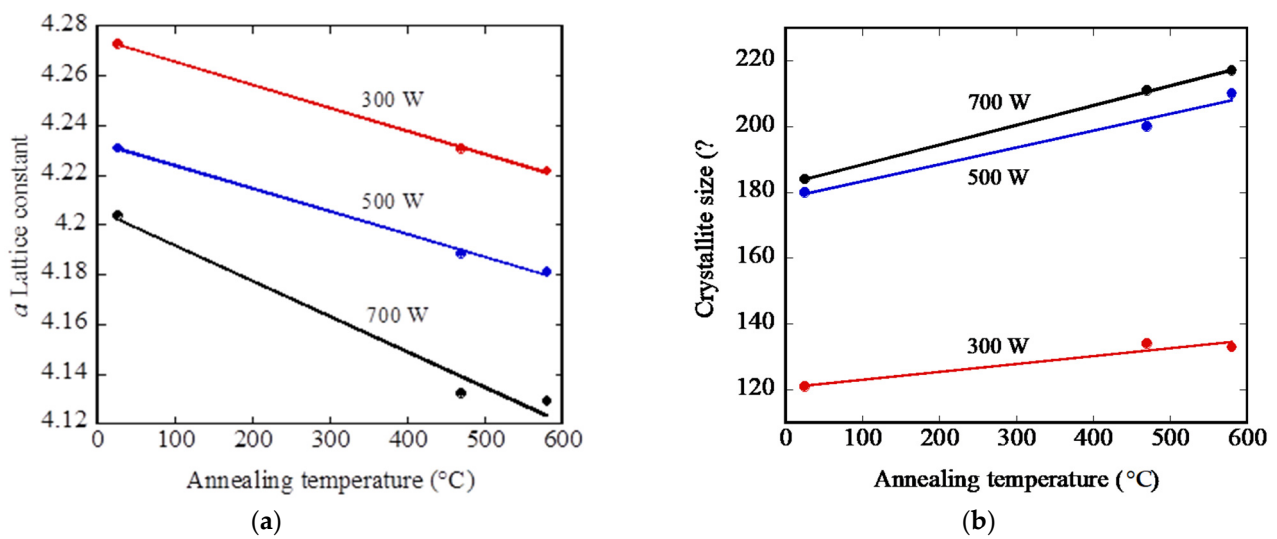
Figure 4. (**a**) Lattice constant vs. annealing T. (**b**) Crystallite size of WN$_x$ films obtained at different deposition powers before and after annealing.

Moreover, a shift of the diffraction lines towards a higher 2θ was observed after the annealing treatment for all the examined films. The shift in XRD diffraction lines, as well as the variation in intensity, could be due to the release of stresses.

The lattice constant decreased with increasing annealing temperature, indicating a relaxation of the structure due to the diffusion out of excess nitrogen atoms by means of a recrystallization process. After annealing at 580 °C, the a-lattice constant values changed from 4.273 Å to 4.223 Å, from 4.231 Å to 4.181 Å and from 4.204 Å to 4.129 Å for the films deposited at 300 W, 500 W and 700 W, respectively.

Only a slight change of crystallite size was observed when the annealing temperature was increased for each analyzed deposition power.

The surface morphology of the film deposited at 500 W after annealing at 580 °C is shown in Figure 5. The surface appears smooth and consisted of rounded small grains, as expected for sputtered films, which generally tended to have a columnar microstructure. Figure 6 shows the surface topography of the film deposited at 700 W before and after annealing treatments. After annealing at 580 °C, the amorphous film was fully crystallized and a segregation of coarse grains was evident. These grains were presumed to be α–W as it results from the X-ray diffraction shown in Figure 3.
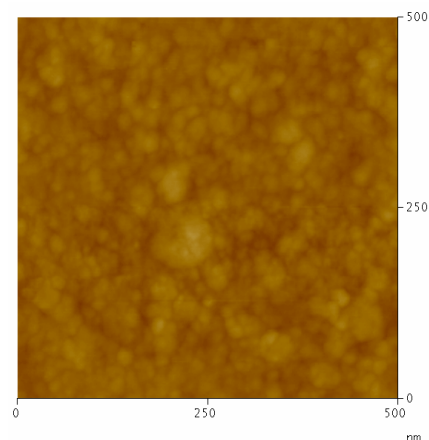

Figure 5. AFM image of 500 W sample after annealing at 580 °C.
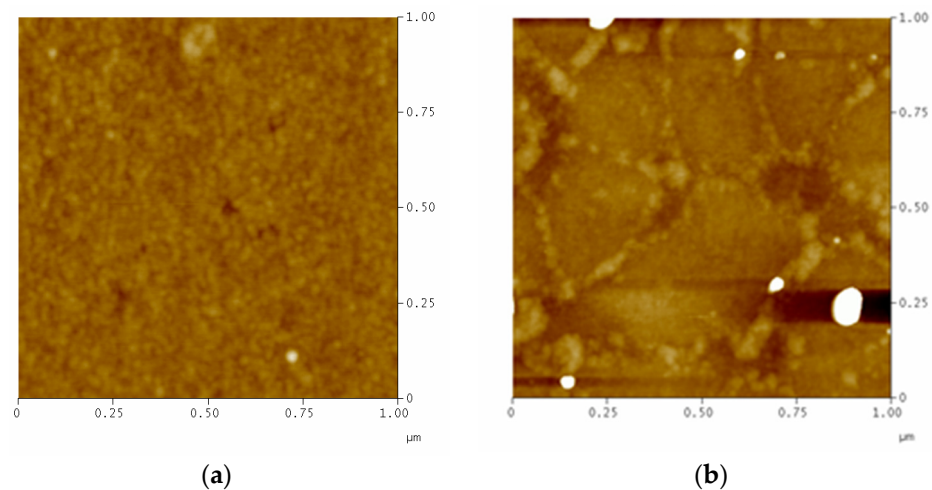
Figure 6. AFM pictures of 700 W WN$_x$ films, (**a**) as deposited and (**b**) annealed at 580 °C.

For metal nitrides that crystallize in cubic structures and ideal "perfect" crystals, first-order Raman scattering is forbidden because there is translational symmetry, q = 0, and all atoms are in centrosymmetric octahedral sites [18]. Nevertheless, sputtered coatings are known to have vacancies that induce distortion in the structure and, as a consequence of this, the Raman spectrum is composed of broadened bands due to disorder and second-order processes. In analyzed samples there was Raman activity, so no stoichiometric cubic nitrides were present. Lattices were expanded by the effect of nitrogen adsorption. The Raman spectra of the as-grown films reported in Figure 7 had three main regions:

- 150–350 cm^{-1} acoustic bands
- 450–650 cm^{-1} optic bands
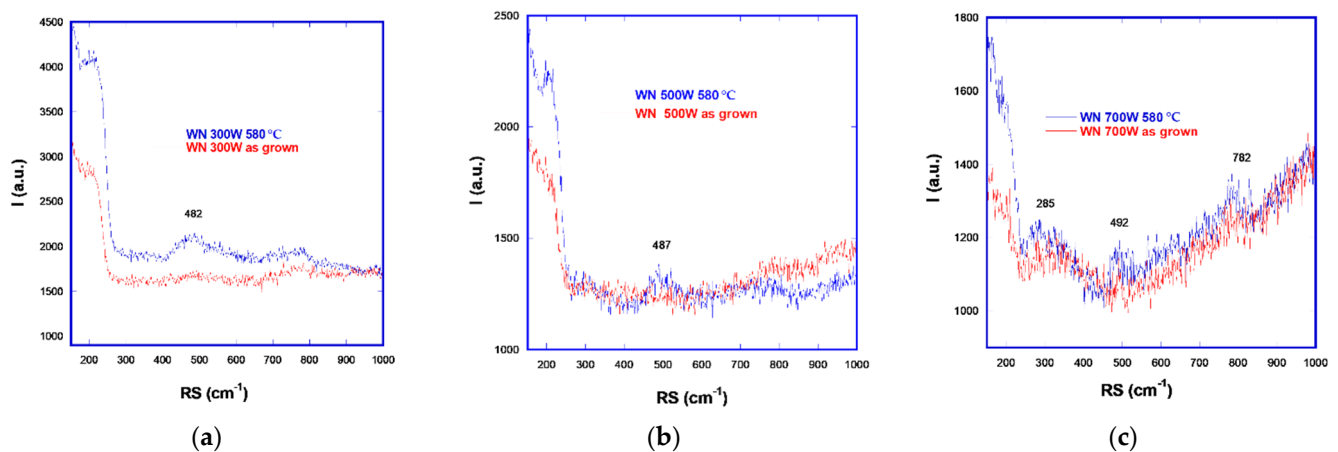- 850–1150 cm^{-1} two phonons contributes.

Figure 7. Micro-Raman before (red line) and after (blue line) annealing at 580 °C for 300 W (**a**), 500 W (**b**), 700 W (**c**).

With regard to the acoustic modes, their intensity is proportional to the dimensions of the crystallites. These bands should have two maxima; in Mo$_2$N they are reported to be 145 cm^{-1} and 205 cm^{-1} [19] Acoustic bands of tungsten nitrides split after annealing into two maxima, as reported in Table 2. In all the as-grown films, there was a unique broad band of low intensity. This behavior can be associated with an increase in crystallite size. In the 700 W film, after annealing the splitting was less accentuated with respect to the other films and a contribute at 187 cm^{-1} was also present, testifying to the contribution of an amorphous phase.

Table 2. Acoustic band splitting of different samples after annealing.

Sample	Acoustic Band Raman Shift First Maximum Position (cm^{-1})	Acoustic Band Raman Shift Second Maximum Position (cm^{-1})
300 W	154	199
500 W	157	206
700 W	161 187	201

　　　　The optical band located at 482 cm^{-1} in the 300 W film, at 487 cm^{-1} in the 500 W film and at 492 cm^{-1} in the 700 W film is due to the stretching of the W-N bond. A film with a higher compressive stress shows a higher frequency shift of this band [20]. The absence of sharp and well-defined peaks could be attributed to local disorder. With the increase in metallic character there Raman activity progressively decreases. Consistently with resistivity measurements, in the 300 W film, after annealing Raman activity increased, the film in fact became more resistive. The 500 W and 700 W films, acoustic bands aside, had an overall comparable Raman activity before and after annealing, consistent with having a similar metallic character.

　　　　As can be seen from the 700 W spectrum, after annealing there was a band at 270–280 cm^{-1} RS that can be attributed to W-O bending, and a band at 780 cm^{-1} that can be attributed to the W-O-W bonds stretching [21]. The presence of such bands, indicative of an oxide phase, could be due to the presence of a tungsten phase originating from disproportion, as already discussed in relation to the XRD results. Metallic nanoparticles oxidize easily. Figure 8 presents a comparison of FTIR reflectance before and after the two annealing steps for all films. The R% decrease is markedly more pronounced in the 500 W and 300 W samples that in the 700 W one.

　　　　FTIR reflectance in the higher-power film remained almost the same, while in both the other films it decreased after annealing. This took place because the content of W$_2$N increases after annealing and the metallic amorphous tungsten nitride clusters crystallize, joining to the prevalent W$_2$N phase lattice, which has a lower FTIR reflectance with respect to an amorphous phase without grain boundaries (which are able to scatter and reduce reflectance). In the high-power case, amorphous WN$_x$ crystallizes as W$_2$N, which could diminish reflectance, but the concomitant formation of metallic tungsten, as also shown by the XRD spectra, balances this decrease by virtue of the higher FTIR reflectance of the metal, denoting an overall effect of reflectance invariance.

　　　　All the films contain simple and multiple tungsten–nitrogen bonds. For a trigonal bi-pyramidal geometry around tungsten, nitrogen ions acting as a ligands can occupy equatorial or axial sites, so the W-N bonds show short (equatorial) and long (axial) distances. The intense bands from 850 cm^{-1} to 1200 cm^{-1} reflect the stretching of the W-N bond, centered at 1097 cm^{-1} in the 300 W and 500 W films and 1086 cm^{-1} in the 700 W film. According to Wang and Andrews [22], the signal at 1097 cm^{-1} can be attributed to the W-N bond stretching in the complex (N-N)$_x$WN, where there is a triple bond W-N [23]. The characteristic signature of the W$_2$N phase is stretching at 870 cm^{-1}, which was not perceived in our film joining in the aforementioned band. Of particular interest are the stretching frequencies of the bridging tungsten bonds evidenced in the inset of Figure 9b. All the films before annealing had a characteristic strong band around 600 cm^{-1} attributable to N-W-N stretching in W complexes with hosted nitrogen molecules, which is less pronounced after annealing, testifying to the evolution toward different N-W-N geometries and types of bond.
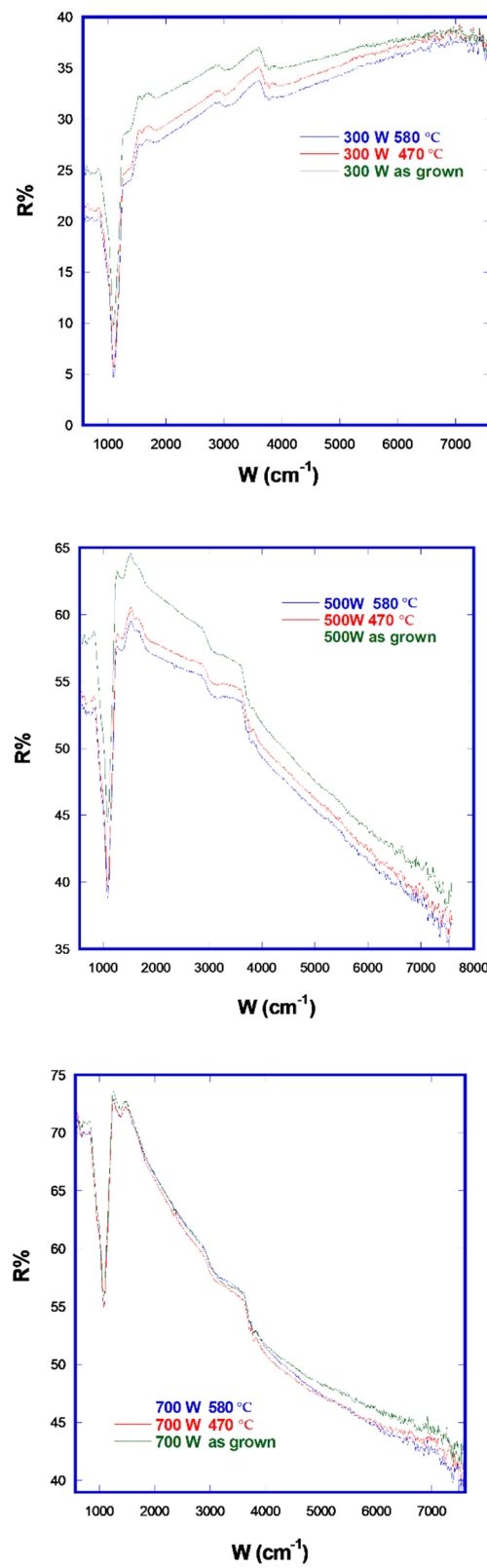
Figure 8. FTIR Reflectance before and after annealing for 300 W, 500 W and 700 W samples.
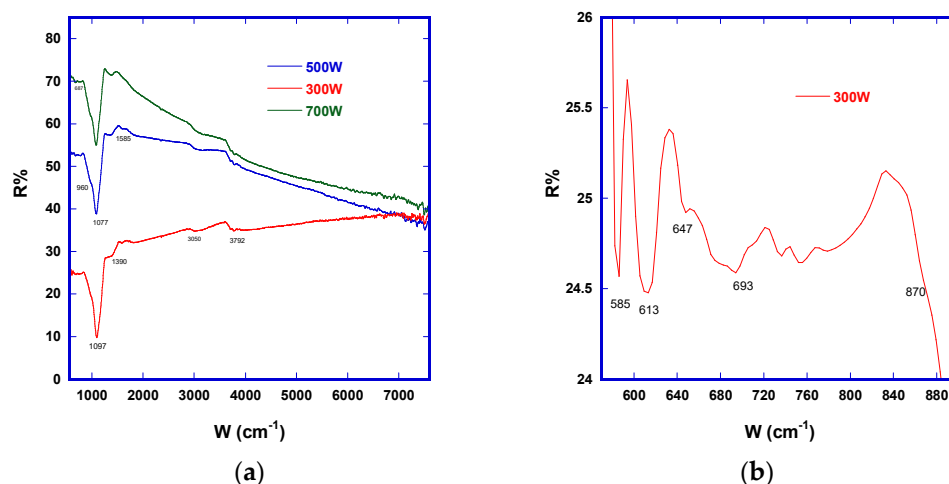
Figure 9. (**a**) FTIR Reflectance comparison; (**b**) 300 W FTIR inset with evidenced signals.

Bands located at 647 cm^{-1} and 693 cm^{-1}, attributed to the bridging nitrogen W-N-W [24], remained almost unchanged after annealing. In the 300 W and 500 W films at 1585 cm^{-1}, there was an N-H bending band. Moreover, at 1390 cm^{-1}, in all the films a scissoring vibration of N-H appeared. The three N-H stretching vibration bands, located at 3089 cm^{-1}, 3128 cm^{-1} and 3253 cm^{-1} in the 300 W, 500 W and 700 W films, respectively, did not change meaningfully after annealing. It is important to note that W hydrazinium complexes, of the kind W—N-NH$_x$, can play a role in the reduction pathway of N$_2$ to form nitrides.

FTIR analysis allows a general consideration of the tungsten nitridation process that takes place in plasma inside a sputtering chamber. Nitrogen reduction to form nitrides (breaking the strong N≡N and forming the azide ion [N=N=N]$^-$), from the chemical point of view, requires extreme conditions. The strong affinity between nitrogen and tungsten provides the driving force to form tungsten nitrides, as a result of a redox reaction between metal and molecular nitrogen. Nitrogen molecules are chemisorbed on tungsten and the triple bond is then progressively weakened. Further reduction of nitrogen proceeds with the formation of an "azo-complex", where each nitrogen atom is bonded to metal atoms and the double bond is hence reduced to a nitride derivative. The whole process requires high temperatures or, as in the biochemical system of nitrogen fixation (where nitrogen is reduced to ammonia derivatives), the aid of an enzyme nitrogenase that uses molybdenum or tungsten cofactors [25]. In a sputtering reactor, high vacuum conditions and ejection of reactive species from the target make nitride synthesis possible at relatively low temperatures. It is reasonable that processes at different powers should determine the formation of different-sized metallic clusters able to adsorb nitrogen and react with it. In fact the arrangement of metal atoms in a metallic cluster can exert a powerful influence on the surface chemical behavior with respect to the adsorption and dissociation of nitrogen. In other words, only a small amount of nitridation occurs by direct reaction with nitrogen-activated ions, while the greater part proceeds by a first stage of gas adsorption from different-sized metallic W clusters, followed by progressive reduction reactions. Hydrogen present in the sputtering chamber, or derived from water molecules, binds itself to the metal clusters and contributes to a minor extent to nitrogen reduction. Another aspect to be considered is that the amorphous W$_x$N, a solid solution of nitrogen in alpha tungsten, can itself be a target, especially at low target powers, and become sputtered itself. Once it has appeared on substrates, this amorphous phase can in turn adsorb other nitrogen and if the temperature is raised it can crystallize in W$_2$N, as already described for the 300 W and 500 W films, or can evolve, expelling excess nitrogen and producing metallic tungsten, like in the 700 W.

Annealing of the 700 W film at 470 °C resulted in a partial crystallization of the amorphous phase, forming a two-phase structure containing the thermodynamic one, W$_2$N.

Further annealing at 580 °C introduced a second modification: together with the W_2N it a second crystalline phase, bcc W, appeared. These modifications progressed with time and temperature because they are based on redox reactions at the interfaces.

Another aspect of the evolution of tungsten nitrides after annealing can be observed when they are part of cermet materials (e.g., with AlN as the ceramic part in absorbing layers of the patented solar double nitride coatings described above [4]). For fabricating a AlN–WN cermet, AlN material (cermet matrix) was produced at a constant cathode power, while WN_x phases dispersed in the matrix were produced by varying the cathode power (with a power value decreasing in a stepwise manner for each layer. When created in this way, a graded cermet has a high metallic content at the start and a low metallic content at the end of process. As for single materials, the same applies as for cermet and the nitridation stage of metallic W influences its stability: barely nitridated materials (700 W) after annealing can dismutate into W and W_2N, while an excess of nitrogen (300 W) undergoes crystalline readjustment with nitrogen release. For the purpose of verifying their stability inside the cermet, thin films of cermet nitrides deposited at the same three representative powers (700 W, 500 W and 300 W) were characterized by means of vibrational analysis before and after annealing. First of all, FTIR reflectance (Figure 10) was found to depend on metallic content; in fact, cermet 700 W had the higher FTIR reflectance and cermet 300 W the lower FTIR reflectance.
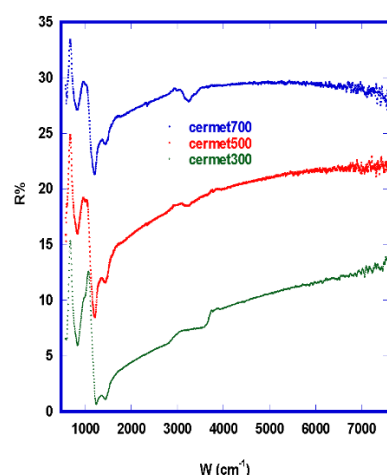

Figure 10. Comparison of FTIR reflectance of cermet samples.

After annealing, there was a decrease in FTIR reflectance for the 500 W and 700 W films, while the 300 W cermet was revealed to be stable (Figure 11). This indicates that matrix protects metallic W_2N particles. Moreover, the NH stretching band at 3225 cm^{-1} disappeared in relation to the proceeding of nitridation process. It is possible that for 700 W cermet film, inside the ceramic AlN matrix, W produced by dismutation was newly exposed to "activated" nitrogen and then newly nitridated.

Wetting experiments were performed to examine the role of electrostatic interactions on annealed WN_x-based thin films. In particular, by using the contact angle made by a droplet of two liquids, polar and nonpolar (water and di-iodomethane), on the solid surface of the samples' basal plane, surface tension was measured, separating the London dispersion (D) and electrostatic components (P). In Figure 12, the water contact angles (WCA°) of the three annealed WN_x samples are reported.
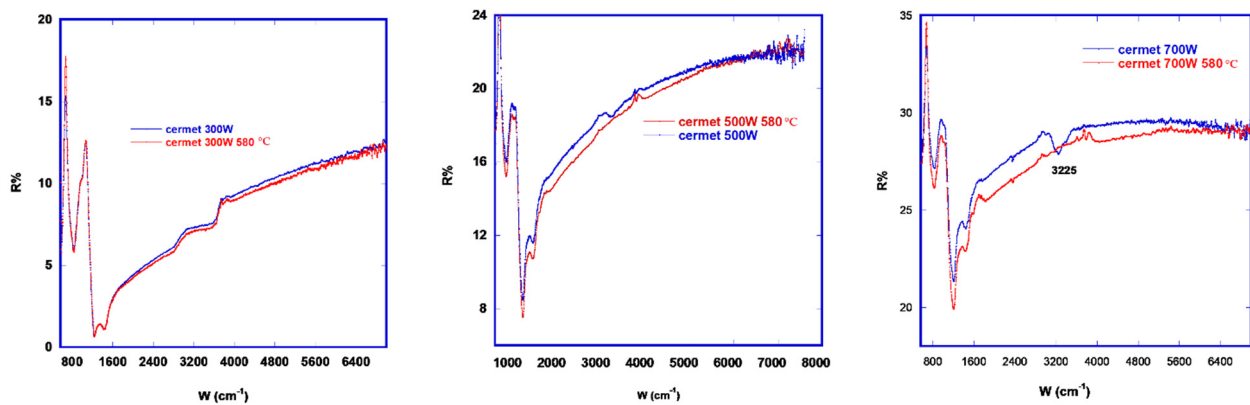
Figure 11. FTIR reflectance of cermet AlN–WN produced at 300 W, 500 W and 700 W.

In Table 3, the WCA° of various WN$_x$ samples and AlN-based cermets are given, including those after annealing.

Table 3. Water contact angle measurements.

Sample	WN300	WN500	WN700	AlN	C300	C500
WCA (°)	73.1 ± 0.9	70 ± 3	74 ± 2	101 ± 2	90.3 ± 4	89.2 ± 2

Surface energies, along with dispersive and electrostatic contributes, are reported in Table 4. Moreover, a further comparison was useful for analyzing wetting behavior: the cermet 500 W before (C500-pre) and after (C500-post) annealing (for estimating the effect of thermal treatment). From the overall set of measurements, it can be outlined that:

- All annealed tungsten nitrides display a similar mild hydrophobic behavior, with a WCA° of around 70°, surface energies around 35 mN/m and a prevalent dispersive force but non-negligible polar contribution to wettability.
- AlN-based cermets containing tungsten nitride nanoparticles are much more hydrophobic with respect to single WN films in terms of the matrix behavior (AlN WCA° > 100°) with surficial energies due to prevalently dispersive forces.

Table 4. Surface energy contributes.

Sample	WN300	WN500	WN700	C500-pre	C50-0post	C300
Surface energy (mN/m)	34.27 ± 1.7	37 ± 2	35 ± 2	39 ± 2	37 ± 1	36.6 ± 1.9
D (mN/m)	22 ± 2	23.9 ± 0.5	24.0 ± 0.9	36	35.3 ± 0.5	35.2 ± 1.2
P (mN/m)	12.8 ± 0.7	13.0 ± 1.7	11.0 ± 1.3	2.7	1.42 ± 0.8	1.42 ± 0.8

A full and detailed analysis can be devoted in a future study to elucidate the frictional properties of tungsten nitrides' basal plane for samples selected as potential electro-catalysts, as an alternative to platinum in HER water-splitting reactions.
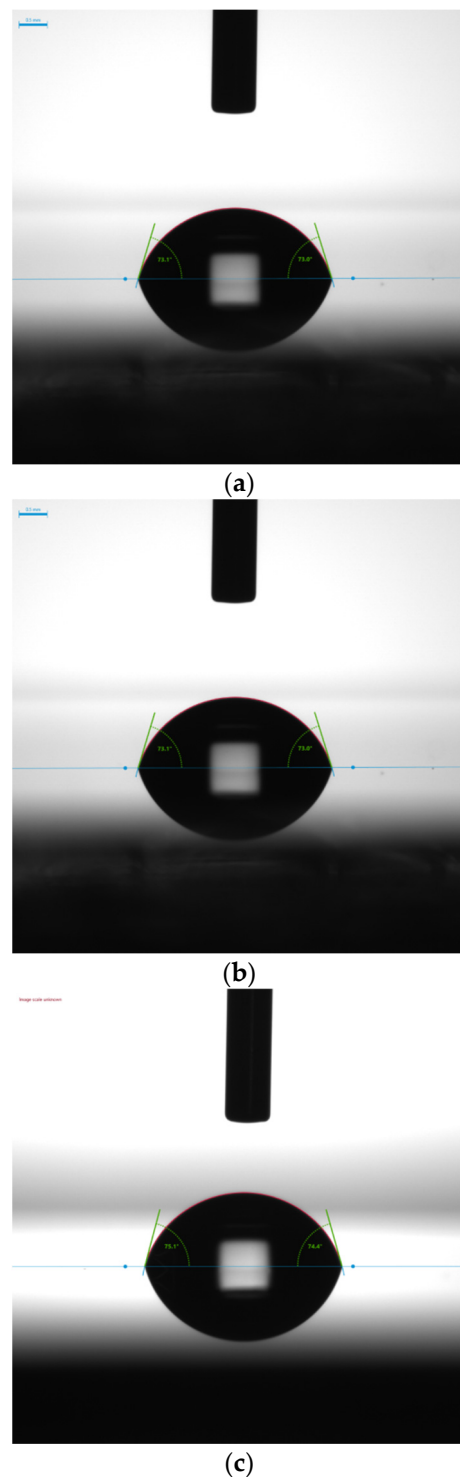
Figure 12. WCA measurements of annealed WN$_x$ samples, (**a**) WN300, (**b**) WN500 and (**c**) WN700.

4. Conclusions

A detailed analysis of the thermal behavior of thin films of tungsten nitride in vacuum was conducted. The main purpose was to assess their viability as constituents of solar coatings, as well as active and robust materials for capacitive energy storage and plasma-facing uses.

Thin films were annealed in vacuum at medium-to-high temperatures (470 °C, 580 °C) and characterized by means of X-ray diffraction (XRD), AFM, micro-Raman, FTIR, UV–VIS– NIR, sheet, surficial energy and wetting angle measurements. The overall set of analyses

evidenced some modifications and differences between the samples (which would be useful for selecting them for specific applications) and, at the same time, provided insight into the mechanism of nitridation occurring in a plasma reactor, where kinetic constraints modulate the reduction of nitrogen to nitride compounds by means of sputtered W metallic clusters' ability to adsorb, form complexes with and react with the strong N_2 triple bond.

After annealing, the 300 W film, which was of poor crystalline quality as deposited, released nitrogen entrapped in the lattice and kept its W_2N structure until 580 °C. In spite of there being no phase transition, there was an increase in sheet resistance but overall optical reflectance stability, even though they were part of the cermet. The 500 W film proved to be the best material for solar thermal applications, having a crystalline structure that remained stable in the desired range and a metallic character that was unmodified by increasing temperature. The 700 W film, whose structure as deposited was almost amorphous, gave raise to modifications after annealing, both as a thin film and as part of a cermet. In facts it crystallized and disproportioned to metallic tungsten and W_2N.

All materials were slightly hydrophobic, with varying wettability with respect to AlN. This behavior can be useful for spheroidizing tungsten nitrides and obtaining good cermet materials. The study of thermal behavior suggested that the thermal evolution of a sputtered WN_x film is strictly dependent on the dimensions of the W clusters obtained during the fabrication process, which in turn depend on process parameters and hence can be controlled. The thermodynamically favored phase, W_2N, tends to form when energy is supplied to the system, but if the nitrogen content is low, a concomitant disproportion can occur with bcc W lattice formation and nitrogen molecule evolution. The redox process seems to be reversible and, in such a direction, a potential catalytic application of thin films as a coating for water-splitting electrodes can be considered.

Institutional Review Board Statement: Not applicable.

Informed Consent Statement: Not applicable.

Conflicts of Interest: The authors declare no conflict of interest.

References

1. Pitz-Paal, R. *Concentrating Solar Power in Future Energy*, 3rd ed.; Elsevier: Amsterdam, The Netherlands, 2020; pp. 413–430. [CrossRef]
2. Antonaia, A.; Castaldo, A.; Addonizio, M.L.; Esposito, S. Stability of W-Al2O3 cermet based solar coating for receiver tube operating at high temperature. *Sol. Energy Mater. Sol. Cells* **2010**, *94*, 1604–1611.
3. Addonizio, M.L.; Antonaia, A.; Castaldo, A.; D'Angelo, A.; Esposito, S.; Ferrara, M.; Guglielmo, A. Highly thermally stable solar selective coatings with W as reflector and WN-AlN as absorber layer. In Proceedings of the E-MRS Spring 2015, Lille, France, 11–15 May 2015.
4. Antonaia, A.; Esposito, S.; Addonizio, M.L.; Guglielmo, A. Solar Selective Absorber Based on Double Nitride Composite Material and Process for its Preparation. U.S. Patent 9,469,896, 18 October 2016.
5. Wang, T.; Yan, Z.; Michel, C.; Pera-Titus, M.; Sautet, C. Trends and Control in the Nitridation of Transition-Metal Surfaces, Acs Catal. 2018, 8, 63–68. *Acs Catal.* **2018**, *8*, 63–68. [CrossRef]
6. Wriedt, H.A. The N-W (nitrogen-tungsten) system. *Bulletin of Alloy Phase Diagr.* **1989**, *10*, 358–367.
7. Akiyama, M.; Morofuji, Y.; Kamohara, T.; Nishikubo, K.; Ooishi, Y.; Tsubai, M.; Fukuda, O.; Ueno, N. Preparation of Oriented Aluminum Nitride Thin Films on Polyimide Films and Piezoelectric Response with High Thermal Stability and Flexibility. *Adv. Funct. Mater.* **2007**, *17*, 458–462. [CrossRef]
8. Addonizio, M.L.; Castaldo, A.; Gambale, E.; Iemmo, L.; Antonaia, A. Influence of process parameters on properties of reactively sputtered tungsten nitride thin films. *J. Vac. Sci. Technol. A* **2012**, *30*, 031506.

9.   Anwar, S. Structural and electrical studies of thermally annealed tungsten nitride thin film. *Adv. Mater. Proc.* **2017**, *2*, 362–366.

10.   Abdelhameed, A.H.; Jacob, W. Deposition of thermally stable tungsten nitride thin films by reactive magnetron sputtering. *Surf. Coat. Technol.* **2019**, *375*, 701–707. [CrossRef]

11.   Yan, H.; Tian, C.; Wang, L.; Wu, A.; Meng, M.; Zhao, L.; Fu, H. Phosphorus-Modified Tungsten Nitride/Reduced Graphene Oxide as a High-Performance, Non-Noble-Metal Electrocatalyst for the Hydrogen Evolution Reaction. *Angew. Chem. Int. Ed.* **2015**, *54*, 6325–6329.

12.   Ma, X.J.; Zhang, W.-B. Tungsten nitride for capacitive energy storage. *ChemistrySelect* **2017**, *2*, 8726–8730.

13.   Tiron, V.; Velicu, I.L.; Porosnicu, C.; Burducea, I.; Dinca, P.; Malinský, P. Tungsten nitride coatings obtained by HiPIMS as plasma facing materials for fusion applications. *Appl. Surf. Sci.* **2017**, *416*, 878–884.

14.   Exner, K.S. Hydrogen electrocatalysis revisited: Weak bonding of adsorbed hydrogen as the design principle for active electrode materials. *Curr. Opin. Electrochem.* **2021**, *26*, 100673.

15.   Jamil, R.; Ali, R.; Loomba, S.; Xian, J.; Yousaf, M.; Khan, K.; Shabbir, B.; McConville, C.F.; Mahmood, A.; Mahmood, N. The role of nitrogen in transition-metal nitrides in electrochemical water splitting. *Chem. Catal.* **2021**, *1*, 802–854.

16.   Wang, S.; Yu, X.; Lin, Z.; Zhang, R.; He, D.; Qin, J.; Zhu, J.; Han, J.; Wang, L.; Mao, H.K.; et al. Synthesis, Crystal Structure, and Elastic Properties of Novel Tungsten Nitrides. *Chem. Mater.* **2012**, *24*, 3023–3028. [CrossRef]

17.   Tian, L.; Bottala-Gambetta, I.; Marchetto, V.; Jacquemin, M.; Crisci, A.; Reboud, R.; Mantoux, A.; Berthomé, G.; Mercier, F.; Sulpice, A.; et al. Improved critical temperature of superconducting plasma-enhanced atomic layer deposition of niobium nitride thin films by thermal annealing. *Thin Solid Film.* **2020**, *709*, 138232. [CrossRef]

18.   Shebova, O.; Soignard, E.; Mamillian, P.F. Compressibilities and phonon spectra of high-hardness transition metal-nitride materials. *High Press. Res.* **2006**, *26*, 87–97. [CrossRef]

19.   Kaindl, R.; Franz, R.; Soldan, J.; Reiter, A.; Polcik, P.; Mitterer, C.; Sartory, B.; Tessadri, R.; O'Sullivan, M. Structural investigations of aluminum-chromium-nitride hard coatings by Raman micro-spectroscopy. *Thin Solid Film.* **2006**, *515*, 2197–2202. [CrossRef]

20.   Andrews, L.; Souter, P.F.; Bare, W.D.; Liang, B. Reactions of Laser-Ablated Mo and W Atoms with dinitrogen: Infrared Spectra of metal nitrides, dinitrides and complexes in solid argon and nitrogen. *J. Phys. Chem A* **1999**, *103*, 4649–4657.

21.   Shigesato, Y.; Murayama, A.; Kamimori, T.; Matsuhiro, K. Characterization of evaporated amorphous WO3 films by Raman and FTIR spectroscopies. *Appl. Surf. Sci.* **1988**, *33–34*, 804–811. [CrossRef]

22.   Wang, X.; Andrews, L. Infrared Spectra, structure and bonding of the group 6 and ammonia M:NH$_3$, H$_2$N-MH, N≡MH$_3$ reaction product in solid argon. *Organometallics* **2008**, *27*, 4885–4891.

23.   Crisholm, M.H.; Folting, K.; Lynn, M.L.; Tiedtke, D.B.; Lemoigno, F.; Eisenstein, O. Nitrido dimers and trimers of tungsten supported by tBuMe2 SiO and CF3Me2CO ligands, respectively. Factors influencing the reductive cleavage of nitriles by tungsten-tungsten triple bonds and an analysis of the structure of the cyclotrimer. *Chem. Eur. J.* **1999**, *5*, 2318–2326.

24.   Cao, Z.; Wan, H.; Zhang, Q. Density functional characterization of N$_2$ dissociation on the step of ruthenium clusters. *J. Phys. Chem.* **2003**, *119*, 9178–9182.

25.   Siemann, S.; Schneider, K.; Oley, M.; Müller, A. Characterization of a Tungsten-Substituted Nitrogenase Isolated from *Rhodobacter capsulatus*. *Biochemistry* **2003**, *42*, 3846–3857. [CrossRef]